Recoil-ion charge-state-resolved electron-production cross sections at 55° for 1 MeV/u C^{5+} on He and Ar

F. Segner, M. Breinig, D. D. Desai, A. Wig, and L. Straus
University of Tennessee, Knoxville, Tennessee 37996-1200
and Oak Ridge National Laboratory, Oak Ridge, Tennessee 37831-6377
(Received 18 December 1995)

Recoil-ion charge-state-resolved doubly differential cross sections for ejecting electrons at ~55° with respect to the incident beam direction in collisions between 1 MeV/u C^{5+} projectiles and Ar and He targets have been measured. Electrons with kinetic energies between 100 and 1250 eV have been detected. A prominent feature in the electron energy distributions is the binary-encounter peak. Experimental results are compared with binary-encounter electron production cross sections obtained using the impulse approximation and with theoretical predictions from many-body classical trajectory Monte Carlo calculations. An enhancement in the fraction of electrons detected with singly charged He recoil ions and a corresponding decrease in the fraction detected in coincidence with doubly charged He recoil ions as a function of the electron energy have been observed near the binary-encounter electron energy. This structure has been predicted by recent many-body classical trajectory Monte Carlo calculations. [S1050-2947(96)01308-X]

PACS number(s): 34.50.Fa, 34.10.+x, 34.80.Bm

I. INTRODUCTION

The emission of electrons into the continuum in fast ion-atom collisions has been the focus of many investigations since the energy and angular distributions of the ejected electrons carry valuable information about the ionizing mechanisms and the structure of the collision partners. The cross sections for producing fast electrons emitted under large angles in fast ion-atom collisions are studied in this work as a function of the electron energy and in coincidence with the target recoil-ion charge state. The energy distributions of electrons that are ejected at ~55° with respect to the beam direction with energies between ~100 and ~1250 eV are measured for 1 MeV/u C^{5+} projectiles colliding with He and Ar targets. The electron spectra reveal different regions associated with specific electron-production mechanisms. In the spectra measured with He and Ar targets, the binary-encounter peak is observed riding on the high-energy tail of the ''soft''-collision peak. In the spectra measured with Ar targets, a distinct peak due to Ar *LMM* Auger electrons is also present.

The soft-collision process [1], which involves dipole-type transitions in glancing collisions, is dominant for the emission of electrons with less than ~10 eV. For fast collisions electron production in soft collisions is well described by the plane-wave Born approximation (PWBA) with an initial bound state and a final continuum state centered at the target. The PWBA describes one-center electron emission, where the target interacts strongly with the electron, whereas the projectile-electron interaction enters as a first-order perturbation. If the projectile velocity is high, the Born approximation is expected to lead to accurate results as long as the projectile charge is not too high.

Binary-encounter electrons (BEE's) are produced in collisions between a target electron and a projectile nucleus when the target's potential becomes negligible compared to that of the projectile. Loosely bound target electrons collide elastically with the projectile nucleus and are ionized into the continuum. For these collisions the impact parameter between the projectile nucleus and the target electron is so small that it is often sufficient to consider only these two partners for the description of the ionized electron's energy and angular distribution. This means that the shape of the screened Coulomb potential of the projectile is the most important parameter determining the distribution of these electrons in energy and emission angle [2]. The target core is essentially a spectator reduced to providing the electron's initial momentum distribution. This initial momentum distribution and the binding energy of the electron in the target must be taken into account by theoretical models since, prior to the collision, the target electron is not actually free. Even though BEE's are produced by violent projectile impact, perturbative methods are often used to describe BEE production involving bare projectiles since they yield results similar to those of higher-order calculations [3].

Two-center electron emission is important in the electron energy range between the soft collisions and the BEE peak. Here experimental cross sections at forward and backward angles often differ considerably from theoretical predictions of the PWBA, especially at intermediate projectile energies. These discrepancies are associated with two-center effects, where the long-range Coulomb forces of both projectile and target atoms play an important role. Continuum-distorted-wave theories describe the final state by a two-center continuum wave function. A particular version, the continuum-distorted-wave–eikonal-initial-state approximation, represents the projectile interaction in the initial state by an eikonal phase. It is suitable to describe electron emission in the combined Coulomb fields of the projectile and target. Experiments measuring the energy and angular distribution of ejected electrons exhibit clear signatures of two-center effects [1,4].

At ~179 eV a large peak is observed in the electron energy spectra measured with Ar targets. It is due to the emission of Ar *LMM* Auger electrons. Fast ions colliding with

atomic targets are likely to produce multiple vacancies in the inner and outer shells and satellite and hypersatellite Auger lines both contribute to the broad peak in the energy spectrum of the emitted electrons [5].

This investigation focuses on the target BEE peak observed at ~55° with respect to the beam direction. Its energy dependence and its dependence on the recoil-ion charge state are studied. Wang *et al.* [6] present a theoretical investigation of the dependence of the binary-encounter electron-production cross section on the charge state of the recoil ion. The ejected electron spectrum is studied in coincidence with the recoil-ion charge state. This approach can also be viewed as qualitatively equivalent to the determination of the impact-parameter range of the collision. Wang *et al.* show that for heavy targets such as Ar, the contribution to the BEE production cross section reaches a maximum at a recoil-ion charge state surprisingly low compared to the highest possible charge state. For He targets an unexpected drop of double ionization and a corresponding local enhancement of single ionization are observed at the binary peak. Wang *et al.* [6] use the many-body classical-trajectory Monte Carlo (*n*CTMC) method for their theoretical investigations. It is particularly suitable when the perturbation is large and the momentum transfer is large, i.e., when a semiclassical description remains valid.

II. THEORY

Many recent papers in theoretical and experimental collision physics have concentrated on BEE production. Different theoretical approaches have been used to calculate the energy and angular distribution of BEE's produced in collisions of bare ions and clothed ions with atomic targets. Examples are the binary-encounter theory [7], the continuum-distorted-wave–eikonal-initial-state approximation [8], the impulse approximation [9], the distorted-wave strong potential Born approximation [10], and the *n*CTMC method [11]. Phenomena investigated experimentally as well as theoretically are the energy shift of the BEE peak [12–14], the anomalous q dependence of the doubly differential cross section (DDCS) [2,15–19], and structure in the energy and angular distributions of BEE's [2,20–22].

In this work the energy distribution of electrons ejected in a direction making an angle of ~55° with the beam direction is measured for 1 MeV/u C^{5+} ions colliding with He or Ar atoms. In these measurements the kinetic energy of the electrons ranges from ~100 to ~1250 eV. The measurements yield the doubly differential cross sections for the production of ''high-energy'' electrons, which are compared with theoretical predictions obtained using the impulse approximation (IA). The IA calculations do not resolve the recoil-ion charge state. For the cross-section calculations we choose the projectile frame as the reference frame and assume that in the projectile frame the target atom approaches the projectile ion with a velocity $\mathbf{v}=v\hat{\mathbf{z}}$. The target electron is scattered through a large angle and leaves the collision with velocity $\mathbf{v}_p$. In the laboratory frame this electron is detected with velocity $\mathbf{v}_l$ making an angle $\theta_l \cong 55°$ with respect to the beam direction.

To calculate the scattering cross section $d^2\sigma/dEd\Omega$ in the projectile frame, we start with the exact result of the impulse approximation with plane-wave final states. The quantum-mechanical impulse approximation represents an attempt to describe many-body scattering approximately in terms of known two-body scattering amplitudes [23]. The impulse approximation assumes that apart from determining the momentum distribution of the bound state, the target potential does not play an important part in the collision. This leads to an expression for the doubly differential scattering cross section [24]

$$\frac{d^2\sigma^{\mathrm{IA}}}{dE_f d\Omega} = \frac{k_f}{v}\,16\pi^4 \int\int\int d^3q\,|\widetilde{\phi}_i(\mathbf{q}-\mathbf{v})\langle \mathbf{k}_f|V_{13}|\psi_{\mathbf{q}}^+\rangle|^2 \times \delta(\mathbf{q}\cdot\mathbf{v}-(E_f+v^2/2-\varepsilon_i)). \tag{1}$$

It contains the exact off-shell two-body T matrix element $T_{fi}(\mathbf{k}_f,\mathbf{q})=\langle \mathbf{k}_f|V_{13}|\psi_{\mathbf{q}}^+\rangle$. Various forms of on-shell approximations (OSA's) can now be invoked. The goal of an on-shell approximation is to replace the δ function in Eq. (1) and to transform the expression for $d^2\sigma/dEd\Omega$ into one that contains only the on-shell, two-body T-matrix element. The on-shell T-matrix element squared, $|T_{if}|^2$, is proportional to the elastic-scattering cross section for free electrons colliding with the projectile ion. The expression for this elastic-scattering cross section is $\sigma_{\mathrm{el}}(E,\cos\theta)=16\pi^4|T_{if}|^2$.

To calculate the production cross section for the high-energy electrons detected in our experiment, an OSA essentially equivalent to the elastic-scattering model of Burch, Wieman, and Ingalls [25] is used. The initial momentum distribution of the electrons $\widetilde{\phi}_i(\mathbf{q}-\mathbf{v})$ is assumed to be strongly peaked around $\mathbf{q}-\mathbf{v}=\mathbf{0}$. Therefore $(\mathbf{q}-\mathbf{v})^2=q^2+v^2-2(\mathbf{q}\cdot\mathbf{v})\cong 0$ and $\mathbf{q}\cdot\mathbf{v}\cong(q^2+v^2)/2$. The δ function in the expression for $d^2\sigma^{\mathrm{IA}}/dE_f d\Omega$ therefore leads to $q^2=k_f^2-2\varepsilon_i$, a constraint on the magnitude of q. For a given k_f, $q^2=q_0^2=k_f^2-2\varepsilon_i$. The expression for $d^2\sigma/dE_f d\Omega$ now becomes

$$\begin{aligned}\frac{d^2\sigma}{dE_f d\Omega} &= \frac{32\pi^4 k_f}{v}\int\int\int d^3q\,|\widetilde{\phi}_i(\mathbf{q}-\mathbf{v})T_{fi}(\mathbf{k}_f,\mathbf{q})|^2 \\ &\quad\times\delta(q^2-k_f^2+2\varepsilon_i) \\ &= \frac{16\pi^4 k_f q_0}{v}\int\int|\widetilde{\phi}_i(\mathbf{q}_0-\mathbf{v})T_{fi}(\mathbf{k}_f,\mathbf{q}_0)|^2 d\Omega_{q_0}.\end{aligned} \tag{2}$$

We now assume elastic scattering and replace $16\pi^4(q_0/v)T_{fi}(\mathbf{k},\mathbf{q}_0)$ by $\sigma_{\mathrm{el}}[E,\cos(\theta_{\mathrm{eff}})]$, with $E=q_0^2/2=k_f^2/2-\varepsilon_i$ and $\cos(\theta_{\mathrm{eff}})=1-|\mathbf{q}_0-\mathbf{k}_f|^2/2q_0^2$. This expression for $\cos(\theta_{\mathrm{eff}})$ preserves the exact momentum transfer during the elastic-scattering event. In the projectile frame the DDCS for the production of BEE's is therefore given by

$$\frac{d^2\sigma}{dE_f d\Omega} = k_f\int\int d\Omega_{q_0}\sigma_{\mathrm{el}}\left(\frac{q_0^2}{2},\,\cos(\theta_{\mathrm{eff}})\right)|\widetilde{\phi}_i(\mathbf{q}_0-\mathbf{v})|^2. \tag{3}$$

The elastic-scattering cross section σ_{el} for free electrons at the projectile ion as a function of electron energy and scattering angle, the initial momentum space wave function of the (scattered) target electron, and the binding energy of the target electron are needed to evaluate Eq. (3). The cross sec-

tion for the elastic scattering of an electron by the spherically symmetric potential of the form $V(r)=Cr^{-1}+V_{sc}(r)$ is given by $d\sigma/d\Omega=|f(\theta)|^2$, with

$$f(\theta)=f_c(\theta)+\sum_{l=0}^{\infty}\frac{1}{k}(2l+1)e^{i(2\eta_l+\delta_l)}\sin\delta_l P_l(\cos\theta). \tag{4}$$

Here $\eta=Cm/\hbar k$,

$$f_c(\theta)=[-\eta/(k\sin^2\theta/2)]e^{2i\eta_0-2i\eta\ln\sin\theta/2},$$

and $\eta_0=\arg\Gamma(1+i\eta)$. For C^{5+} in the ground state $V(r)$ is given by

$$V(r)=-\frac{e^2}{r}e^{-2Zr/a_0}\left(1+\frac{Zr}{a_0}\right)-\frac{(Z-1)e^2}{r}, \tag{5}$$

where Z is the nuclear charge of the hydrogenic ion and a_0 is the Bohr radius. To find $d\sigma/d\Omega=|f(\theta)|^2$, δ_l is calculated by solving the radial equation numerically for $V(r)=Cr^{-1}$ and for $V(r)=Cr^{-1}+V_{sc}(r)$ using the Numerov algorithm.

The initial momentum-space wave function of the scattered target electron is of the form $g_{nl}(k)Y_{lm}(\hat{\mathbf{k}})$. The target gases are He and Ar. For the ground state of the He atom, Hartree-Fock wave functions are used to calculate $g_{10}(k)$. The binding energy of the electron in the ground state of He is 24.59 eV [26]. For Ar targets we assume that only the loosely bound $n=3$ electrons contribute to the BEE production cross section. Again Hartree-Fock wave functions are used to numerically calculate $g_{3s}(k)$ and $g_{3p}(k)$ for Ar. The binding energy of the $3s$ electron in Ar is 29.24 eV and the binding energy of the $3p$ electron is 15.85 eV [26]. The doubly differential cross sections for BEE production at 55° in the laboratory frame for He and Ar targets are first calculated in the projectile frame and then transformed to the laboratory frame.

Figure 1(a) shows the result of our calculations for collisions between a 1 MeV/u C^{5+} ion and He targets. The calculated DDCS $d\sigma/dEd\Omega$ in the laboratory frame has a maximum of ~635 eV electron energy. This differs from the peak position predicted by Rutherford scattering at 55° by ~90 eV. The measured peak is shifted towards lower energy. Free electrons detected at 55° in the laboratory frame, after elastically scattering off the ion approaching with velocity v, would have kinetic energy $T=2mv^2\cos^2(55°)=722$ eV. Figure 1(b) shows the total DDCS $d\sigma/dEd\Omega$ in the laboratory frame for collisions between 1 MeV/u C^{5+} ions and an Ar target and the contributions of the $3s$ and the $3p$ electrons to the total DDCS. The BEE peak for an Ar target is broader than the BEE for a He target. The DDCS has a maximum at ~615 eV electron energy. The peak shift is ~105 eV towards lower energy.

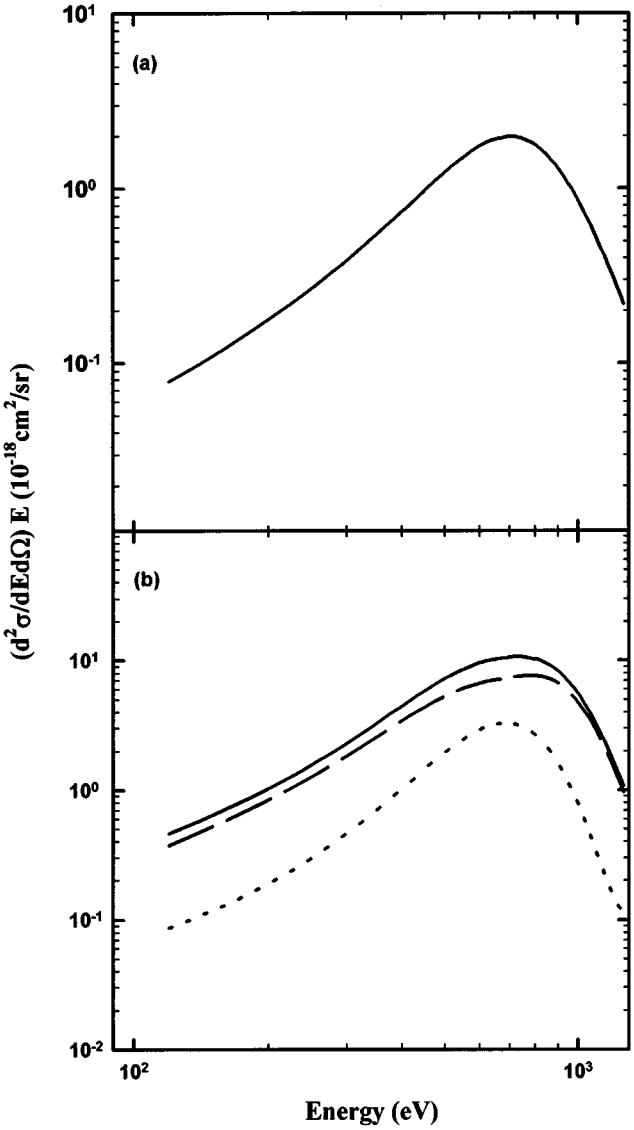

FIG. 1. (a) DDCS, multiplied by energy, for electron emission at 55° in collisions of 1 MeV/u C^{5+} with He, calculated in the impulse approximation. (b) DDCS, multiplied by energy, for electron emission at 55° in collisions of 1 MeV/u C^{5+} with Ar (solid line), calculated in the impulse approximation, and contributions of the $3s$ (dotted line) and $3p$ (dashed line) electrons to the total DDCS.

III. EXPERIMENT

The EN Tandem Van de Graaff accelerator located at the Oak Ridge National Laboratory is used to produce a 12-MeV beam of C^{5+} ions. Before entering the experimental chamber the beam passes through two circular 3/4-mm-diam apertures situated 1.32 m apart for collimation. A 1-mm-diam skimmer aperture is located 10 cm downstream from the second aperture. In the experimental chamber the C^{5+} projectiles collide with He or Ar gas in a gas cell that is located approximately 40 cm from the skimmer. The gas cell is surrounded by four different spectrometers. One of the spectrometers is a time-of-flight (TOF) recoil-ion charge-state analyzer. The other three spectrometers are electron energy analyzers: a double-pass cylindrical mirror analyzer (CMA) and two 30° parallel-plate analyzers. This multispectrometer apparatus (MSA), shown in Fig. 2, is enclosed in a μ-metal housing for magnetic shielding and resides in a vacuum chamber that is pumped by an oil diffusion pump and a turbo pump. The base pressure is less than 10^{-7} Torr. After passing through the gas cell the ions pass through a charge-state analyzer, which can be used to separate ions exiting from a collision in the gas cell according to their exit charge state. Approximately 2 m downstream from the gas cell the ions are col-

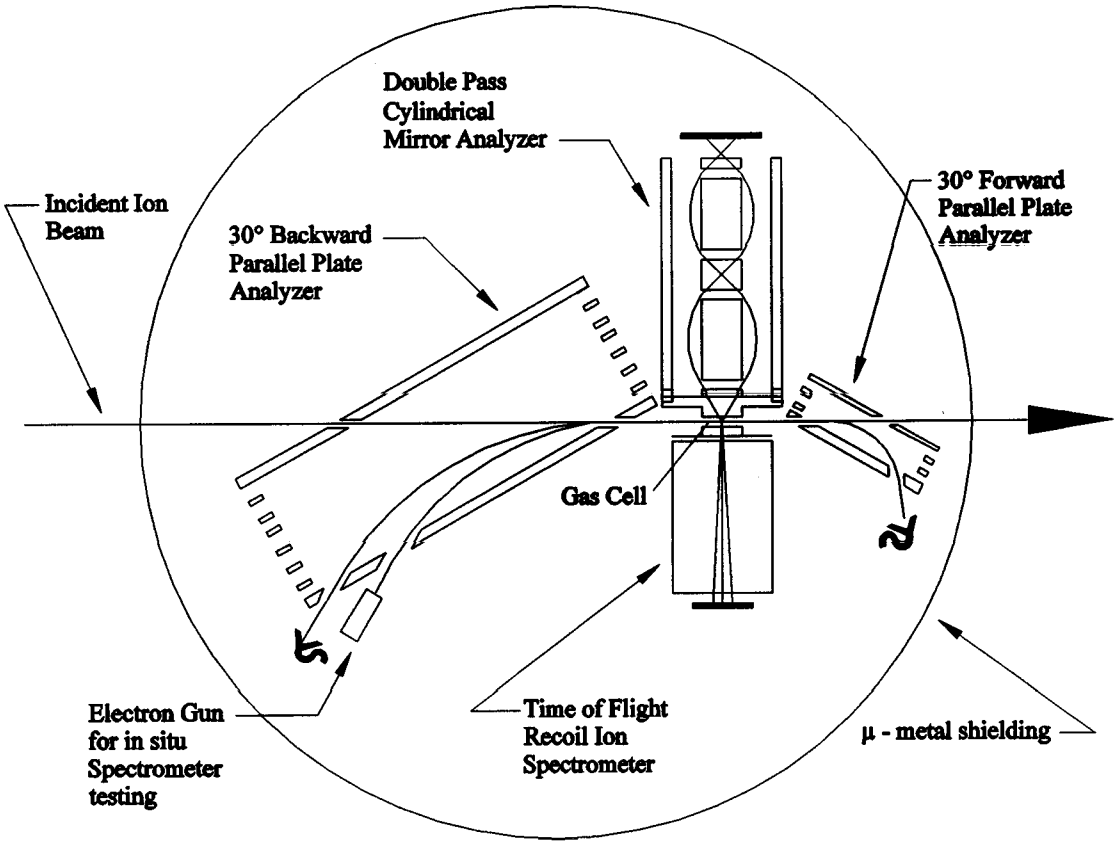

FIG. 2. Schematic diagram of the multi-spectrometer apparatus.

lected in a Faraday cup or registered individually with a multidynode electron multiplier.

The MSA is used to energy analyze electrons ejected under single-collision conditions and to determine the associated recoil-ion charge state. Coincidence experiments, such as the experiments described here, often place conflicting demands on the experimental apparatus. Target recoil ions are born with very low energy and move slowly. They need to be accelerated by an electric field in the target region towards a recoil-ion detector. Higher electric fields generally result in higher recoil-ion detection efficiencies. Electrons are very light particles and are strongly affected by an electric field in the target region. High electric fields here will prevent them from reaching their detector or will distort their trajectories through the electron analyzer. Therefore only weak electric fields ($\lesssim$ 10 V/cm) can be used in the target region to accelerate recoil ions and the detection efficiency is quite low. It is desirable to measure the energy distribution of the ejected electrons with high-energy resolution, high angular resolution, and good detection efficiency, but it is necessary to find a good compromise concerning these properties of the apparatus. To measure the energy distribution of electrons emitted at 55° with respect to the beam direction in coincidence with the target recoil-ion charge state, we have designed a cylindrical mirror analyzer with good transmission efficiency, at the expense of energy and angular resolution, to be a part of the multispectrometer system. All metal parts of the CMA are machined from aluminum to ensure that no residual internal stray magnetic fields alter the trajectories of electrons through the CMA. In order to avoid inhomogenuities of the electric field between the two cylinders, all entrance and exit slits are covered with a ''one-dimensional grid.'' Single metal wires are attached parallel to the cylinder axis to the walls of the inner cylinder. No wires are attached perpendicular to the cylinder axis. Electrons reaching the two-dimensional position-sensitive detector (PSD) of the CMA have to pass through four of these grids at an angle of $\sim$45° with respect to the cylinder axis and perpendicular grids severely reduce the transmission probability.

The recoil-ion charge state is determined by measuring the time difference between an electron reaching the PSD of the CMA and an ion reaching the microchannel plate detector of the TOF spectrometer, which consists of a source region, an acceleration region a, and a field free drift region. The regions are separated from each other by carbon fiber grids made from $\sim$7.3-μm-diam carbon fiber filaments with better than 99% transmission per grid. A small extraction voltage is applied across the gas cell, which results in an electric field of $\sim$6 V/cm. The use of two ion acceleration stages allows us to keep the electric field in the gas cell low to minimize the deflection of electrons born here. By choosing the voltages across the gas cell and the acceleration region in the correct ratio, we achieve space focusing, i.e., ions born at different positions in the source region arrive at the detector after the same flight time [27].

In the experiments described here the total beam current is collected in a Faraday cup and from this current the total number of incident ions is determined. For a given number of projectiles passing through the gas cell, we count the total

number of electrons of a given energy that are detected on a chosen area of the PSD and the number of electrons detected in coincidence with recoil ions of charge state q.

IV. DATA ANALYSIS

A. Ar data

Measurements are made at two different target gas pressures: 2 and 3 mTorr. The energy distributions of all electrons, detected independently of any coincidence requirement and measured at different times and with different pressures in the gas cell, agree within statistical error when normalized per incident ion per mTorr. Background contributions due to electrons produced by scattered projectile ions striking the gas cell, apertures, or other surfaces are therefore negligible. This is expected since the ion beam is well collimated and the MSA is well aligned.

From the raw energy distributions of electrons measured in coincidence with target recoil ions of charge state 3^+, 4^+, and 5^+, contributions due to random coincidences are subtracted. The resulting true coincidence spectra are then normalized and checked for consistency. Again they agree within statistical error. To normalize the coincidence spectra, the recoil-ion detection efficiency must be known. It is determined by fixing the CMA voltage so that only Ar LMM Auger electrons can pass the analyzer and by determining the number of electrons reaching the PSD and the number of true coincidences between electrons and recoil ions for some time interval t_1. Each Auger electron is produced in coincidence with a target recoil ion. By dividing the number of true coincidences by the number of Auger electrons detected, the recoil-ion detection efficiency is found to be 0.04 ± 0.002.

B. He data

Measurements are made at three different target gas pressures: 8, 10, and 12 mTorr. The total number of electrons and the number of electrons detected in coincidence with He^+ and He^{2+} recoil ions are measured as a function of electron energy. Random coincidences are subtracted from the raw coincidence spectra. The normalized true coincidence spectra all agree within statistical error. However, the energy distributions of all electrons detected without coincidence requirement measured at different times do not agree within statistical error. This is probably caused by a small amount of contamination in the target gas. Contributions due to contamination are not observed in the true coincidence spectra since the detection of a He recoil ion is required. The energy distribution of all electrons ejected is therefore obtained by adding the normalized distribution measured in coincidence with He^+ and He^{2+} recoil ions.

C. Cross sections

To obtain absolute cross sections from the measured total electron yields per incident ion per mTorr, the number of target atoms per cm^2, the transmission function of the CMA, and the detection efficiency for transmitted electrons must be known. In order to obtain absolute cross sections from the measured electron–recoil-ion coincidence yields, the recoil-ion detection efficiency must also be known. The number of target atoms per cm^2 per mTorr is computed using the ideal gas law and the effective gas-cell length. The probability that an electron, produced in a collision with kinetic energy T and emission angle θ, will pass through the CMA and will reach the selected area of the PSD with the analyzer voltage at V is found using a computer simulation of the CMA. Electrons are born in the region where the ion beam interacts with the target gas. To calculate the probability that an electron produced in this region reaches the selected area of the PSD, the program incorporates the exact dimensions of the analyzer, including all apertures and slits. The simulation generates a uniform distribution of points in velocity space in a volume V_v using a random-number generator. These velocities are assigned to a uniform distribution of randomly chosen starting positions in a volume V_r, where the ion beam intersects the target gas. Electrons not within V_v and V_r definitely cannot reach the detector. The program first assumes that the electric field in the region between the cylinders of the CMA is that of an infinitely long cylindrical capacitor and then adds correction terms to incorporate the influence of fringe fields. It calculates the trajectory for each electron using the Runge-Kutta algorithm and determines if the electron will reach the selected area of the PSD. The velocity components of the transmitted electrons yield the energy and angular resolution of the CMA and the analyzer constant. From the full width at half maximum of a plot of the number of transmitted electrons versus energy for a fixed analyzer voltage, the energy resolution is determined to be $\Delta E/E \cong 5\%$, and from the full width a half maximum of a plot of the number of transmitted electrons versus emission angle with respect to the beam axis, $\Delta\theta$ is determined to be $\sim 8°$ at $\theta = 55°$. The electron detection efficiency depends on several different variables. If electron detection is independent of any coincidence requirements, it depends on the detection efficiency of the PSD, the transmission of the grids, and for a small CMA, as is used here, it also depends in detail on how the apertures and slits are machined. This number is therefore obtained from a second experiment. An electron gun is used to produce beams of 500- and 800-eV electrons and the cross section for the elastic scattering of electrons at 55° on Ar is measured with the CMA. The electron detection efficiency is found by comparing the measured results with published elastic-scattering cross sections [28].

Relative uncertainties in the cross section measured as a function of electron energy are mainly due to statistical errors and to small fluctuations of the target gas pressure in the gas cell. Statistical errors always increase due to background subtraction. Absolute errors are due to the error in the determination of the effective gas-cell length, the error in the transmission function of the CMA, and the error in the electron and recoil-ion detection efficiencies. These errors are quadratically propagated and yield an absolute error in the measured cross section of $\sim 21\%$.

V. RESULTS AND CONCLUSIONS

Recoil-ion charge-state-resolved doubly differential cross sections for ejecting electrons at $\sim 55°$ with respect to the incident beam direction in collisions between 1 MeV/u C^{5+} projectiles and Ar and He targets have been measured. The absolute magnitude and energy dependence of the total doubly differential cross sections for He and Ar targets, indepen-

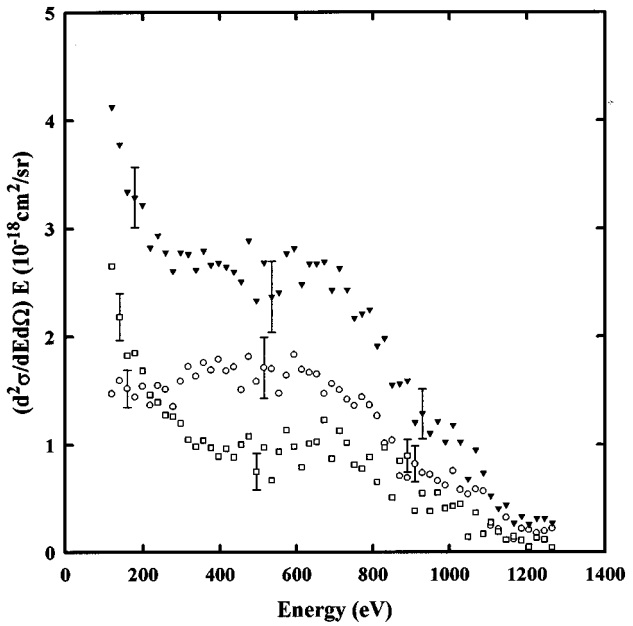

FIG. 3. DDCS, multiplied by energy, for electron emission at ~55° with respect to the beam direction, in coincidence with He^+ (squares) and He^{2+} (circles), for 1 MeV/u C^{5+} on He. The triangles show the total DDCS, independent of recoil-ion charge state.

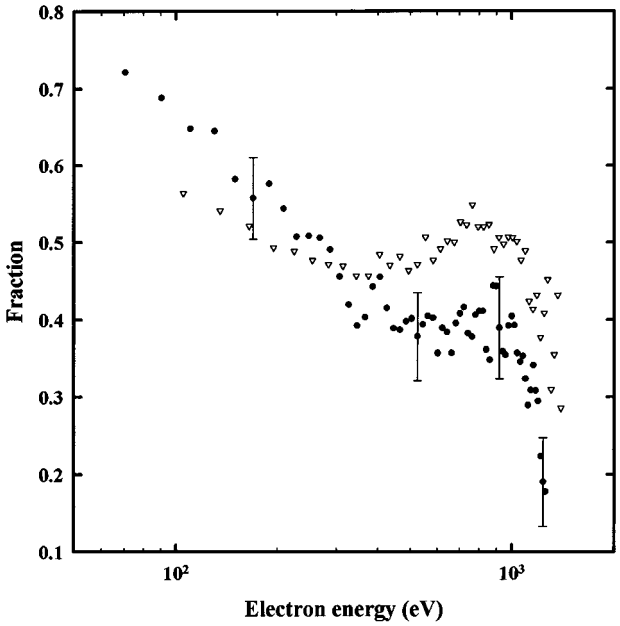

FIG. 4. Fraction of electrons emitted at ~55° in coincidence with the production of a He^+ recoil ion for 1 MeV/u C^{5+} on He (theory, triangles; experiment, circles).

dent of recoil-ion charge state, are compared with theoretical predictions obtained using the impulse approximation. From the coincidence cross sections the fraction of electrons emerging in coincidence with selected target recoil-ion charge states is computed. For He targets these fractions are compared with the theoretical predictions by Wang *et al.* obtained from *n*CTMC calculations.

A. He data

Figure 3 shows the doubly differential cross section for electron emission at ~55° with respect to the beam direction in coincidence with He recoil-ion charge states 1^+ and 2^+ for C^{5+} projectiles on He. The error bars in our figures indicate relative errors. The probability for projectile ionization is very low, so that no projectile electrons are observed. The total electron-production cross section is therefore the sum of the 1^+ and 2^+ coincidence cross sections. Charged particles can ionize a neutral target by inducing optically allowed (dipole) and nondipole transitions [29]. Nondipole transitions require large energy and momentum transfers and are often termed ''hard'' collisions. A well-known example is the production of BEE's generated by head-on collisions between a massive particle and an electron. In Fig. 3 the BEE peak rests on a smoothly decreasing background of target electrons directly ionized via dipole-type transitions. Most of these BEE's are produced in coincidence with He^{2+}. The fraction of electrons produced with He^+ is shown Fig. 4. It decreases rapidly as the electron energy increases. However, as the electron energy approaches the BEE peak energy, the single-ionization fraction increases again, reaching a local maximum right at the binary peak. Accordingly, the double-ionization fraction has a local minimum at the binary peak. A similar behavior of the single and double ionization was predicted by Wang *et al.* [6] for electrons emitted at 20° in 2.4 MeV/u Xe^{21+} on He collisions using the *n*CTMC method. Wang has repeated these *n*CTMC calculations for the collision system 1 MeV/u C^{5+} on He studied in this experiment. His results are presented in Fig. 4 overlaid on the experimental results. The qualitative agreement is quite good. In their paper Wang *et al.* interpreted the decrease in double ionization near the binary peak in terms of a two-step sequential removal mechanism. When one electron is removed, the second electron is left in the electric field of the He^{2+} nucleus. The momentum distribution of such an electron has a broader width. In BEE production the portion of the momentum distribution being probed is at the center of the Compton profile. Double ionization decreases because a broader Compton profile has a lower center. We favor a different model. Ionization of neutral targets by charged ions depends on the projectile charge Z and the collision velocity v [30]. The important parameter governing ionization is Z/v. For $0.2 \lesssim Z/v \lesssim 1$ double ionization of the target is dominated by a two-step process in which the projectile interacts with each of the target electrons independently. Therefore, in the Z/v regime probed in this experiment, a two-step removal is likely to be responsible for double ionization over the whole measured electron energy range. In Fig. 3 the doubly differential electron production cross sections are varying smoothly with energy. We do not observe strong resonances. Under those circumstances a larger cross section often means that the process can happen over a larger impact-parameter range. High-energy target electrons produced via dipole-type transitions are produced in small impact-parameter collisions. BEE production does not require a close collision between two nuclei, only a close collision between the target electron and the projectile nucleus. Thus a high-energy free electron can also be produced in relatively large ''internuclear'' impact-parameter collisions, if the probability of finding

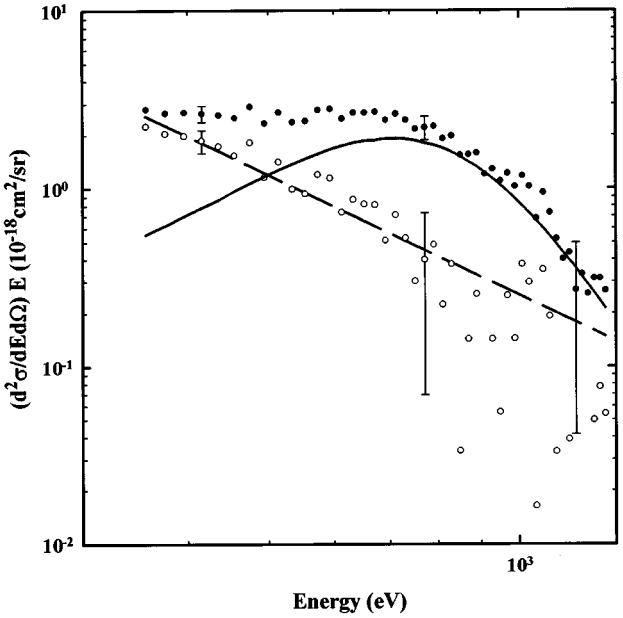

FIG. 5. Comparison of the measured DDCS (full circles), multiplied by energy, for electron emission at ~55° for 1 MeV/u C^{5+} on He, and the results of our IA calculations (solid line), multiplied by 0.7. When the theoretical results are subtracted from the data, the remaining background (open circles) decreases approximately as $E^{-3.35}$ (dashed line).

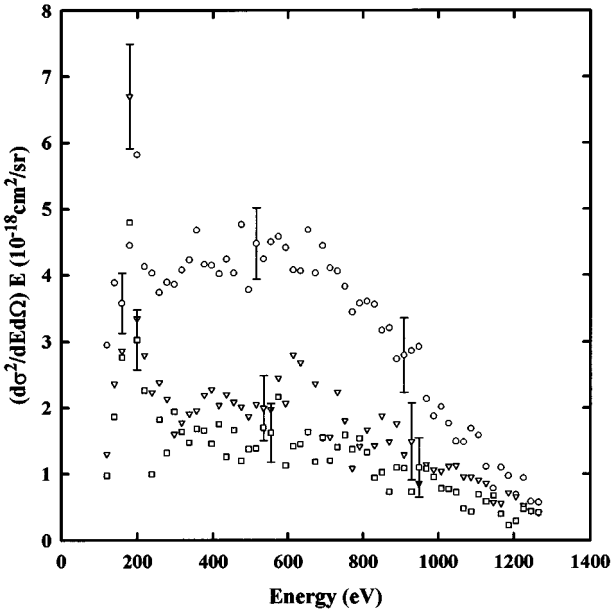

FIG. 6. DDCS, multiplied by energy, for electron emission at ~55° with respect to the beam direction, in coincidence with Ar^{3+} (circles), Ar^{4+} (triangles), and Ar^{5+} (squares), for 1 MeV/u C^{5+} on Ar.

the target electron at these distances is nonzero. Since double ionization of the target is expected to increase rapidly as the impact parameter of the collision decreases, the larger impact-parameter range for the BEE production process therefore leads to a decrease in the double-ionization fraction at the binary peak.

Figure 5 shows the doubly differential electron-production cross section and the results of our IA calculations multiplied by 0.7. These calculation reproduce the shape and position of the BEE peak quite well. When the theoretical curve is subtracted from the measured data, only a background due to target electrons ionized via dipole-type transitions remains. Several investigations show that the cross section for ionizing via this type of transition decreases approximately as $1/E^x$ in the energy range over which our BEE production cross-section calculations are valid [1,3]. Figure 5 shows the background remaining after substraction of the theoretical curve decreases as $\sim 1/E^x$ (with $x=3.25$). The calculation overestimates the magnitude of the experimentally measured cross section. This may be expected since it does not incorporate the change in binding energy due to multiple ionization of the target. Most of the BEE's are observed in coincidence with He^{2+}. However, the experimentally measured cross section has an absolute error of more than $\pm 20\%$, so it is not possible to make a detailed quantitative comparison.

B. Ar data

Figure 6 shows the doubly differential cross section for electron emission at ~55° with respect to the beam direction in coincidence with Ar recoil-ion charge states 3^+, 4^+, and 5^+. In addition to the BEE peak resting on a smoothly decreasing background of target electrons, a peak due to Ar LMM Auger electrons is observed at ~179 eV electron energy. Nearly all of the BEE's are produced in coincidence with target recoil-ion charge states 3^+, 4^+, and 5^+. When the sum of the doubly differential cross sections measured in coincidence with these exit charge states is subtracted from the total doubly differential cross section, only a smoothly decreasing background remains. Figure 7 shows the fractions of the total number of electrons emitted at ~55° that are detected in coincidence with Ar recoil ions of charge states 3^+, 4^+, and 5^+, respectively. Except near 179 eV, where we find the signature of Ar LMM Auger electrons, the fraction of electrons detected in coincidence with Ar^{4+} recoil ions does not show a peak and increases slightly with electron energy. The fraction detected in coincidence with the lower target recoil-ion charge state 3^+ increases as the electron energy approaches the binary-peak energy and reaches a maximum at the binary peak. Above the binary-peak energy it decreases rapidly. In contrast, the fraction detected in coincidence with the higher recoil-ion charge state 5^+ decreases slightly as the electron energy approaches the binary-peak energy and then starts increasing above the binary-peak energy. BEE's are detected in coincidence with surprisingly low recoil-ion charge states, clearly showing that a process other than the dipole-type transitions is responsible for the production of these high-energy electrons. In contrast, Ar LMM Auger electrons are primarily detected in coincidence with the higher recoil-ion charge states 4^+ and 5^+. The measured peak is composed mainly of unresolved satellite lines. Ion-atom collisions that produce an inner-shell hole most often also leave multiple vacancies in the outer shells.

No recoil-ion charge-state-resolved theoretical predictions are available for the 1 MeV/u C^{5+} on Ar system. Figure 8 shows the total doubly differential cross section, independent

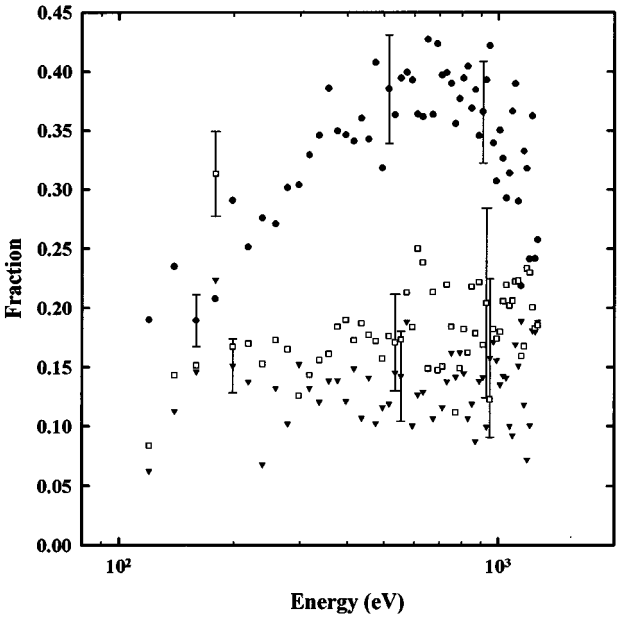

FIG. 7. Fraction of electrons emitted at ~55° and detected in coincidence with Ar^{3+} (circles), Ar^{4+} (squares), and Ar^{5+} (triangles) recoil ions for 1 MeV/u C^{5+} on Ar.

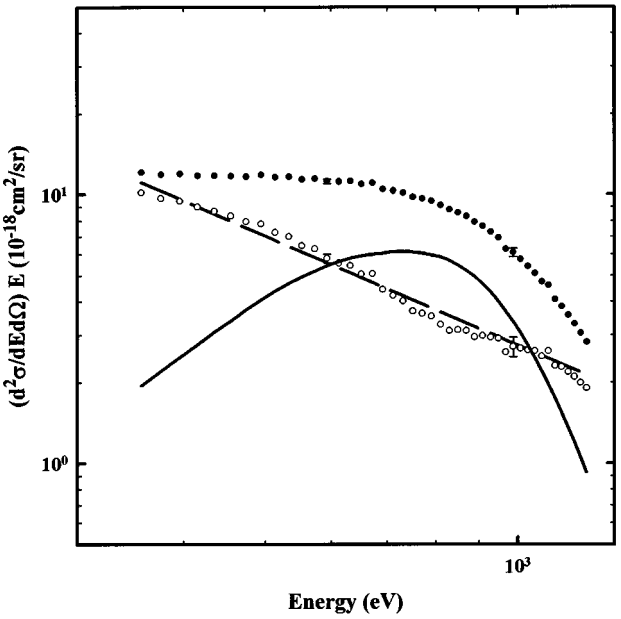

FIG. 8. Comparison of the measured DDCS (full circles), multiplied by energy, for electron emission at ~55° for 1 MeV/u C^{5+} on Ar, and the results of our IA calculations (solid line), multiplied by 0.6. When the theoretical results are subtracted from the data, the remaining background (open circles) decreases approximately as $E^{-2.35}$ (dashed line).

of recoil-ion charge state, and the results of our IA calculations, which are multiplied by a factor 0.6 for the Ar target. Again the calculations seem to reproduce the shape and position of the BEE peak quite well. When the theoretical curve is subtracted from the measured data, only the Auger peak and a background of target electrons ionized in soft collisions remain. This background decreases as $1/E^x$ (with $x=2.35$). Again, the calculations overestimate the magnitude of the measured cross section.

C. Summary

Total BEE production at 55° can be reasonably well modeled using the elastic-scattering model as an on-shell approximation to the IA. Except for a background decreasing as $1/E^x$ in the energy region of the BEE peak, this approximation predicts the shape and peak position of the BEE peak well. The height of the measured BEE peak agrees with the height of the calculated peak within ~30%.

BEE's are produced in coincidence with lower recoil-ion charge states more frequently than electrons of the same kinetic energy produced by other ionization mechanisms. The average impact parameter for producing these high-energy electrons via the binary-encounter process is probably larger than for producing them via other ionization processes. The *n*CTMC calculations of Wang *et al.* predicting the fraction of He^+ and He^{2+} recoil ions for 1 MeV/u C^{5+}+He agree qualitatively with the data observed in coincidence with electrons emitted at 55°.

ACKNOWLEDGMENTS

This work was supported in part by the National Science Foundation and by the U.S. Department of Energy, Office of Basic Energy Sciences, Division of Chemical Sciences, under Contract No. DE-AC05-84OR21400, with Martin Marietta Energy Systems, Inc., and by the UTK Exhibit, Performance and Publication Expense Fund.

[1] N. Stolterfoht, D. Schneider, J. Tanis, H. Altevogt, A. Salin, P. D. Fainstein, R. Rivarola, J. P. Grandin, J. N. Scheurer, S. Andriamonje, D. Bertault, and J. F. Chemin, Europhys. Lett. **4**, 899 (1987).

[2] C. Kelbch, R. Koch, S. Hagman, K. Ullmann, H. Schmidt-Böcking, C. O. Reinhold, D. R. Schulz, R. E. Olson, and D. Kraft, Z. Phys. D **22**, 713 (1992).

[3] D. H. Madison and E. Merzbacher, in *Atomic Inner Shell Processes*, edited by B. Crasemann (Academic, New York, 1975), p. 1.

[4] P. D. Fainstein, V. H. Ponce, and R. D. Rivarola, J. Phys. B **24**, 3091 (1991).

[5] P. Richard, in *Atomic Inner Shell Processes* (Ref. [3]), p. 73.

[6] J. Wang, R. E. Olson, H. Wolf, J. Shinpaugh, W. Wolff, and H. Schmidt-Böcking, J. Phys. B **26**, L457 (1993).

[7] T. F. M. Bonsen and L. Vriens, Physica **47**, 307 (1970).

[8] P. D. Fainstein, V. H. Ponce, and R. D. Rivarola, Phys. Rev. A **45**, 6417 (1992).

[9] D. H. Jakubassa-Amundsen, Phys. Rev. A **49**, 2634 (1994).

[10] J. Macek and K. Taulbjerg, J. Phys. B **26**, 1353 (1993).

[11] D. R. Schultz and R. E. Olson, J. Phys. B **24**, 3409 (1991).
[12] D. H. Lee, P. Richard, T. J. Zouros, J. M. Sanders, J. L. Shinpaugh, and H. Hidmi, Phys. Rev. A **41**, 4816 (1990).
[13] A. D. González, P. Dahl, P. Hvelplund, and P. D. Fainstein, J. Phys. B **26**, L135 (1993).
[14] W. Wolff, H. E. Wolf, J. L. Shinpaugh, J. Wang, R. E. Olson, P. D. Fainstein, S. Lencinas, U. Bechthold, R. Herrmann, and H. Schmidt-Böcking, J. Phys. B **26**, 4169 (1993).
[15] P. Richard, D. H. Lee, T. J. M. Zouros, J. M. Sanders, and J. L. Shinpaugh, J. Phys. B **23**, L213 (1990).
[16] R. E. Olson, C. O. Reinhold, and D. R. Schulz, J. Phys. B **23**, L455 (1990).
[17] C. O. Reinhold, D. R. Schulz, and R. E. Olson, J. Phys. B **23**, L591 (1990).
[18] C. O. Reinhold, D. R. Schulz, and R. E. Olson, Nucl. Instrum. Methods Phys. Res. Sect. B **56**, 271 (1991).
[19] T. J. M. Zouros, P. Richard, K. L. Wong, H. I. Hidmi, J. M. Sanders, C. Liao, S. Grabbe, and C. P. Bhalla, Phys. Rev. A **49**, R3155 (1994).
[20] C. Kelbch, R. E. Olson, S. Schmidt, and H. Schmidt-Böcking, J. Phys. B **22**, 2171 (1989).
[21] C. O. Reinhold, D. R. Schulz, R. E. Olson, R. Koch, and H. Schmidt-Böcking, Phys. Rev. Lett. **66**, 1842 (1991).
[22] J. L. Shinpaugh, W. Wolff, H. E. Wolf, U. Ramm, O. Jagutzki, H. Schmidt-Böcking, J. Wang, and R. E. Olson, J. Phys. B **26**, 2869 (1993).
[23] M. R. C. McDowell and J. P. Coleman, *Introduction to Theory the of Ion-Atom Collisions* (North-Holland, Amsterdam, 1970).
[24] J. Wang, C. O. Reinhold, and J. Burgdörfer, Phys. Rev. A **44**, 7243 (1991).
[25] D. Burch, H. Wieman, and W. B. Ingalls, Phys. Rev. Lett. **30**, 823 (1973).
[26] K. D. Sevier, At. Data Nucl. Data Tables **24**, 323 (1979).
[27] W. C. Wiley and I. H. McLaren, Rev. Sci. Instrum. **26**, 1150 (1955).
[28] R. D. DuBois and M. E. Rudd, J. Phys. B **9**, 2657 (1976).
[29] J. Wang, J. H. McGuire, and J. Burgdörfer, Phys. Rev. A **51**, 4687 (1995).
[30] J. H. McGuire, N. Berrah, R. J. Bartlett, J. A. R. Samson, J. A. Tanis, C. L. Cocke, and A. S. Schlachter, J. Phys. B **28**, 913 (1995).
[31] S. T. Manson, L. H. Toburen, D. H. Madison, and N. Stolterfoht, Phys. Rev. A **12**, 60 (1975).